A&A, 703, A306 (2025)
https://doi.org/10.1051/0004-6361/202556317

Astronomy & Astrophysics

The elliptical configuration of the X-ray-emitting intracluster medium

Graziella di Tullio Zinn*

Department of Astronomy, Yale University, P. O. Box 208101, New Haven, CT 06520-8101, USA

Received 8 July 2025 / Accepted 12 October 2025

ABSTRACT

Context. The morphology of the hot gas X-ray images within galaxy clusters provides indications about the formation, populations, mergers, and evolution of clusters in connection with their dynamical state.
Aims. The aim of this investigation is to search for a link between one or more basic morphological parameters describing the elliptical configuration of intracluster medium (ICM) X-ray contours and the dynamical state of the parent cluster.
Methods. We used the 2021 X-CLASS Survey Catalogue of X-ray-detected galaxy clusters. We selected the sample of 982 spectroscopically confirmed clusters, and visually inspected the shape and orientation of their hot gas X-ray contours. We recognized a variety of morphological structures that could lead to a certain dynamical state. A more detailed analysis was carried out by fitting ellipses to the X-ray digitized contours of a subsample of 105 clusters, already classified in the literature as dynamically relaxed, dynamically non-relaxed, or dynamically intermediate.
Results. Some correlations have been found among our measurements of ellipticity (ϵ) for ICM X-ray contours and the classified dynamical state of the parent cluster. The majority of the relaxed clusters present an increase in ellipticity outward from the cluster center; exceptions include a conspicuous number of clusters with essentially ICM constant ellipticity. In contrast, most of the non-relaxed clusters have ellipticity profiles decreasing outward, with fewer exceptions. Moreover, the total variation in ellipticity ($\Delta\epsilon$) tends to be smaller for the X-ray contours of relaxed clusters than for those of non-relaxed clusters, including maximum ellipticity values. Intermediate clusters overlap with both groups. Similar results are found by applying the selected morphological parameters to ICM X-ray contours available in the literature from other X-ray observations.

Key words. galaxies: clusters: intracluster medium

1. Introduction

The current modeling for clusters of galaxies describes their structures as being composed of a large dark matter halo (∼85%), filled with hundreds to thousands galaxies and permeated by hot intracluster gas. X-ray observations of clusters of galaxies have consistently revealed the diffused presence of the hot intracluster medium (ICM) (see Sarazin 1986; Biviano 2000, for historical reviews). There are two main theories about the origin of the ICM: 1. a primordial origin before the formation of galaxies (Gunn & Gott 1972) 2. an ejection origin from galaxies within the clusters, mostly by supernovae explosions, and AGN feedback (De Young 1978). Both models explain some of the properties of the intracluster hot gas, for example the high ICM mass (primordial component) and the presence of metals (galactic ejection component). The medium is a superheated plasma ($T \sim 10^8$ K) that consists of fully ionized hydrogen and helium, with traces of heavier elements, including iron as a function of redshift (Mantz et al. 2017).

This intracluster hot gas reveals itself through the emission of strong X-ray radiation, mainly by the Bremsstrahlung process that can be observed using X-ray telescopes, from the oldest NASA Uhuru X-ray satellite (1972) to the more recent NASA Chandra X-ray spacecraft (1999) and ESA XMM-Newton satellite (1999). Despite its extremely low density (10^{-3} particles cm^{-3}), the ICM is a major baryonic component of a galaxy cluster (∼12%) greater in mass than the stellar matter (∼3%) (Pratt et al. 2019).

Because of its higher mass, the measurements of the ICM from X-ray emissions with the analysis of its density distribution are fundamental steps to reveal the nature of clusters, their dynamical state, formation process and evolution. The ICM also gives insights into how ordinary matter and dark matter are distributed throughout the Universe, taking into account that clusters of galaxies are the largest bound and most massive structures in the Universe 10^{12}–10^{14} solar masses; (Böhringer et al. 2017). However, high quality optical imaging is still used to study cluster morphology, because photometric indicators are obtained more easily from large optical surveys, than the X-ray morphological parameters obtained from high resolution pointed X-ray observations, which are extremely costly (Casas et al. 2024).

Optical and X-ray images have revealed that galaxy clusters present a range of observational properties delineating cluster dynamical states that vary from very relaxed to extremely non-relaxed and disturbed, due to their formation processes and merging histories. Other fundamental properties of clusters, such as their mass and temperature, also appear to be related directly or indirectly to their dynamical state, which provides constraints for their total mass measurements and for cosmological models (Mantz et al. 2022). Throughout the literature, various properties of clusters and some morphological features of the ICM, have been considered quantifying indicators of the cluster dynamical state. Vice versa different metrics, both observational and within simulations used to probe the cluster dynamical

* Corresponding author: graziella.zinn@yale.edu

state, are quantifying different core properties (Cerini et al. 2023; Haggar et al. 2024, and references therein). Investigating the dynamical state of galaxy clusters becomes of paramount importance to understand their nature.

For the present study we are mostly interested in the identification of one or more possible basic morphological parameters, derived from the elliptical configuration of ICM X-ray contours, that could lead directly to a quick preliminary identification of the dynamical state of clusters and their stage of evolution. The motivation to focus on the elliptical ICM X-ray configuration came from the results that the author obtained with a similar analysis previously done on the isophotes of elliptical galaxies, in a variety of environments including galaxy clusters (di Tullio 1978, 1979). In addition, more recent studies have shown that the isophotal shapes of clusters' central elliptical galaxies exhibit coherent alignment with the shape of their parent cluster. These studies argue that the phenomenon may be connected with the cluster formation and evolution, including the cluster ellipticity traced by the satellite distribution (Huang et al. 2016). Clusters do appear more or less elongated when projected on the sky and their shapes have been reconstructed as triaxal rather than spherical, consistent with the Lambda cold dark matter (ΛCDM) paradigm (Sereno et al. 2018, and references therein).

In this ellipsoidal model a 2D elliptical shape approximation may well illustrate the dynamical state of a cluster (Shankar & Khatri 2021) since a cluster looking not relaxed in a 2D X-ray map would look even more disturbed in a 3D representation. In this perspective, our approach to measure the 2D elliptical configuration of the ICM may become one of the quantifying indicators for the overall dynamical state of the parent cluster since ellipticity parameters can provide insights of its dynamical shape and presence of substructures in connection with its evolution history. The ellipticity of galaxy clusters has been considered an intrinsic independent cluster feature (Flin 1984).

A large number of studies, both observational and within cluster simulations, have been published to propose quantitative measurements for the relaxation or non-relaxation state of galaxy clusters (see Sect. 2 for details and references). We used their classification as the source for our initial grouping of a selected cluster sample, following their division into relaxed, non-relaxed, and intermediate, as a calibration for our proposed ellipticity morphological parameters.

From optical and near-IR photometric imaging, combined with high spatial resolution X-ray observations, clusters are generally considered candidates for dynamical relaxation if they do not show any clear sign of disruption from ongoing merger activities, for example large substructures in galaxy distribution or large asymmetries in ICM X-ray contours. In relaxed clusters, hot gas and galaxies are expected to settle into the potential well, reaching a state of hydrostatic equilibrium and stabilizing the cluster (Tchernin et al. 2020). Therefore, the relaxed dynamical state should be reflected in a more symmetric galaxy and ICM density distribution. On the contrary non-relaxed clusters have not yet settled in a stable configuration, but are still showing signs of disruption or even active mergers, with the display of ICM density perturbations and asymmetries. After an extensive merger event, it would take up to billions of years for a cluster to restore a dynamical state of relaxation in correlation with the halo mass change (Zhang et al. 2022). Clusters in the intermediate category are the bridge between the other two groups. Their partially regular X-ray morphology may still show some effects of previous merging, such as rippling in the X-ray gas density contours (Heinrich et al. 2024). Our present study concentrates on comparing some ellipticity parameters of ICM contours associated with these three categories of clusters.

The structure of the paper is as follows. In Section 2 we present our sample of clusters selected from the X-CLASS Survey Catalogue, including their dynamical state classification published by various other authors. In Section 3 we describe our procedure to extract ellipticity parameters from the X-ray ICM contours provided by the XMM Cluster Archive Super Survey. In Section 4 we present the resulting ellipticity measurements for each cluster, focusing on some specific ellipticity parameters. In Section 5 we compare our parameters with similar data available in the literature or with data extracted by applying our procedure of fitting ellipses to other published X-ray contours. In Section 6 we summarize and discuss our findings. In Section 7 we present our conclusions about an ICM ellipticity criterion for cluster relaxation.

2. Sample selection

2.1. Galaxy clusters in XMM-Newton Archive

Our sample of clusters was selected from the X-CLASS Survey Catalogue published in 2021 (Koulouridis et al. 2021). The catalog is based on the XMM-Newton archival observations publicly available until August 2015. We chose this catalog because of their homogeneous large list of X-ray detected galaxy clusters, the extended redshift range (up to $z \sim 1.5$) over a wide area of the sky ($\sim$269 deg^2 across), the high galactic latitude sky ($|b| > 20°$), and the uniform quality of the ICM X-ray density contours, up to the projected radius of 3.5 arcminutes (exposure times of 10 and 20 ks). At first our interest concentrated on the 982 objects of the catalog list that are spectroscopically confirmed clusters. A visual inspection revealed a variety of morphological structures, from fairly uniform and symmetrical to fragmented, possibly related to the dynamical state of the cluster and not apparently connected with the cluster redshift. This interpretation would support a scenario of cluster formation and evolution of their dynamical state, as an ongoing process since the early Universe.

Figure 1 offers a sample of eight galaxy clusters with ICM X-ray density contours and spectroscopic redshifts provided by the X-CLASS catalog. They are examples of the larger cluster population contained in the catalog, with different morphological structures in the contours of constant X-ray surface brightness.

More regular and less regular cluster morphology with the presence of substructures appear to be somewhat independent from the cluster redshift, even taking into account the distance effect. They are probably related to the evolution history and the dynamical state of the cluster. We investigate these morphological features further in the following sections, starting with a subsample of 105 galaxy clusters (Sect. 2.2). We apply to them a procedure to extract their underlying elliptical X-ray morphology (Sects. 3 and 4).

2.2. Subsample of clusters with dynamical state classification

To carry out a more detailed analysis of the various ICM morphological structures, we have selected a subsample of 105 objects among the spectroscopically confirmed galaxy clusters in the X-CLASS catalog. They will be our calibration reference for a dynamical classification based on ICM contour ellipticity. In addition to having ICM X-ray contours available from

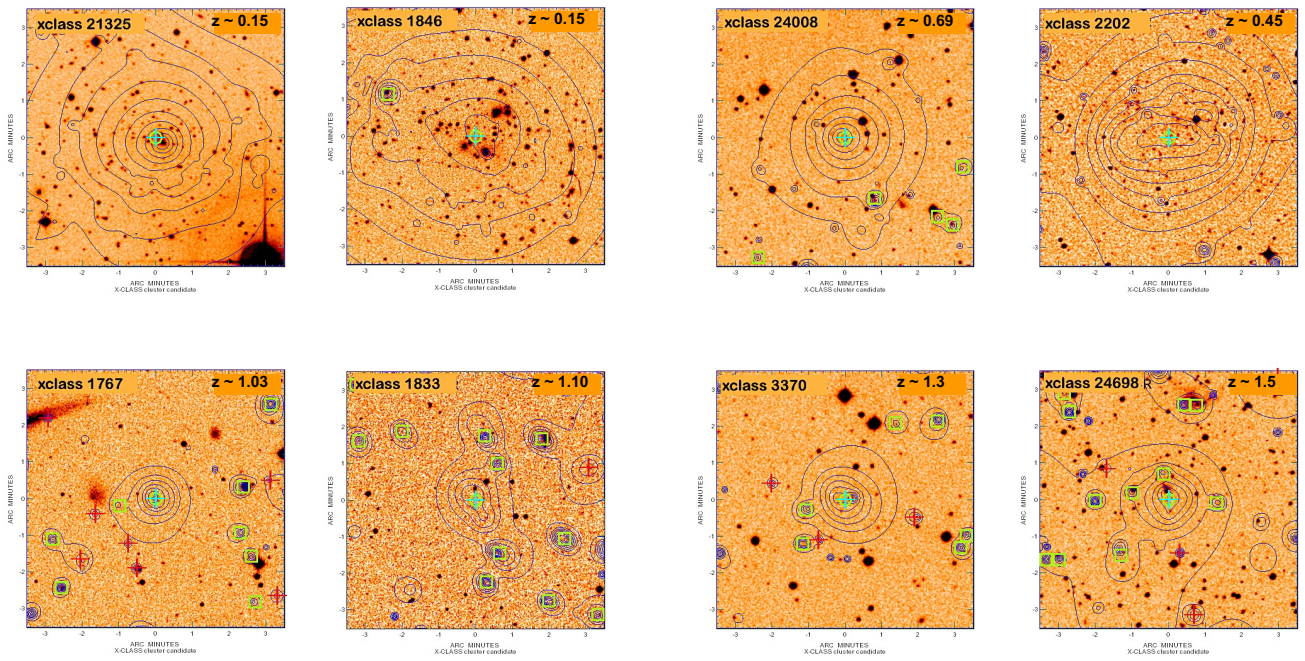

Fig. 1. XMM-Newton ICM X-ray contours of constant X-ray surface brightness, superimposed onto DSS2-*r* band images of the parent galaxy cluster. The green circles represent extended sources and the green squares refer to point sources. The eight clusters are grouped in pairs that belong to four increasing intervals of cosmological redshifts ($z \sim 0.15; 0.4 < z < 0.7; 1 < z < 1.1; 1.3 < z < 1.5$).

the XMM Cluster Archive Super Survey, these clusters have their dynamical state already classified and published by different authors. The classification includes dynamically relaxed clusters (43 objects), dynamically non-relaxed (47), and dynamically intermediate (15).

Tables A.1, A.2, and A.3 give the lists of these three separate categories with their ID numbers, coordinates, and spectroscopic redshifts. The last column refers to the names and works of the various authors who provided the cluster dynamical classification. They used a variety of morphological parameters, mostly based on observations provided by the Chandra X-ray telescope.

Several of the listed authors, although with different methods, focus on symmetry, concentration, peakness, smoothness, and alignment with the global center, for cluster X-ray images and density contours (Schmidt & Allen 2007; Govoni et al. 2009; Mantz et al. 2015; Parekh et al. 2015; McDonald et al. 2019; Yuan et al. 2022; Heinrich et al. 2024; Ebeling et al. 2025; Véliz Astudillo et al. 2025).

Clusters that are dynamically relaxed present a more symmetrical and smoother morphology, with a sharper X-ray density concentration toward the center. In particular, some of the authors emphasize the alignment between the brightest central galaxy (BCG) and the peak of the cluster X-ray flux. Relaxed clusters are expected to have good alignment and concentric density contours (Casas et al. 2024; Ebeling et al. 2025; Véliz Astudillo et al. 2025).

Another sign of dynamical relaxation that has been considered is the presence of a cool core, revealed by a prominent peak in X-ray surface brightness and a systematic central temperature drop. The dynamics of relaxed clusters promotes a more uniform ICM distribution, allowing a shorter cooling time of the undisturbed gas at the cluster's center (Hudson et al. 2010; Heinrich et al. 2024; Ebeling et al. 2025). On the other hand, mergers can disrupt cool core clusters, thus playing a vital role in cluster evolution, from dynamically relaxed to highly disturbed clusters. Mergers can also create multiple subcomponents. They can be detected through optical imaging of mass distribution inside clusters, or from X-ray observations of ICM shock waves (Tempel et al. 2017; Łokas 2023). Since galaxy clusters are dominated by dark matter, mass distribution can be measured by gravitational lensing. Relaxed clusters display a more uniform mass distribution that can produce better defined gravitational lenses, without the heavy distortion caused by substructures present in non-relaxed clusters. In contrast, relaxed clusters reveal only a single core with defined rounder contours.

In some cases, the elliptical shape of X-ray images has been measured to test the effects of the underlying dark matter gravitational potential on the dynamical state of clusters (Schmidt & Allen 2007; Mantz et al. 2015; Parekh et al. 2015; Harvey et al. 2019; Yuan et al. 2022; Cerini et al. 2023). These studies of mass concentration have found that clusters with the lowest total ellipticity appear to be dynamically relaxed, while highest ellipticity belongs to the dynamically unrelaxed. However, their data show a considerable overlap between the two groups of clusters, and total ellipticity has not been considered a useful indicator for separating relaxed from non-relaxed clusters. This result is of particular interest for our present study of ellipticity measurements for ICM X-ray contours. In Section 5 we present a comparison with our ellipticity indicators for the clusters in common.

3. Procedure for fitting ellipses to the ICM X-ray contours

We employed the following method for fitting ellipses and for extracting ellipticity morphological parameters from ICM X-ray contours in the galaxy clusters of our sample. The website of the XMM Cluster Archive Super Survey[1] provides Digitized Sky

[1] https://xmm-xclass.in2p3.fr

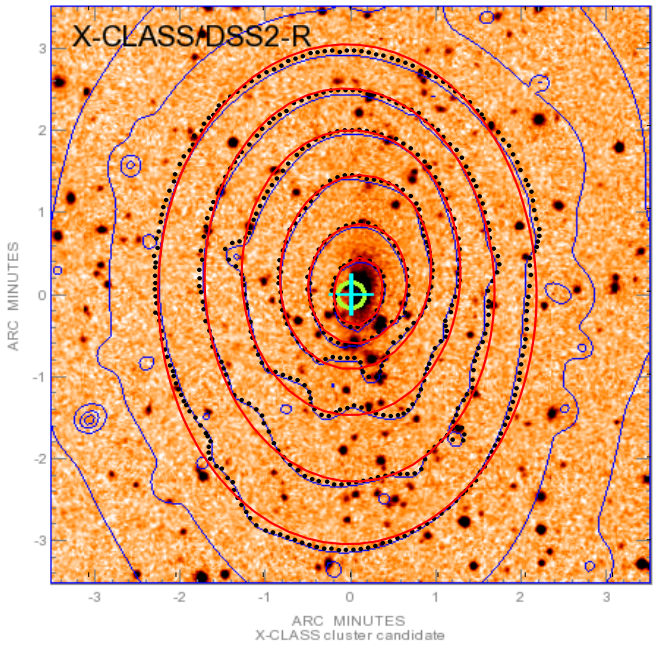

Fig. 2. Our digitized contours (black dots with fitted red ellipses) are superimposed onto the ICM X-ray contours (blue lines) provided by the XMM Cluster Archive for the dynamically relaxed cluster X-CLASS 1701 (see Table A.1 for dynamical classification).

Survey II R images of the clusters with ICM X-ray contours superimposed. According to the website, the X-ray contours of constant X-ray surface brightness were wavelet constructed from co-added images from the PN, M1, and M2 detectors, which cover the 0.5–2 keV range. We downloaded the images in PDF format and then digitized the contours using the Web Plot Digitizer software[2]. This digitation yielded approximately 50–80 points along the circumference of the smallest contours and 300 or more for the largest. The points closely followed the contours, with only minimal smoothing by hand when we had to remove the X-ray point sources in the field (identified with green squares) that were affecting the contours. Using the least-squares method, we fitted ellipses to the digitized contours, as shown in Fig. 2.

From the semimajor (a) and semiminor axes (b) of the fitted ellipses, the ellipticity ϵ ($\epsilon = 1 - b/a$) was calculated. From the uncertainties in ellipse parameters, the one-sigma error in ϵ was calculated. Comparisons of the contours with the fitted ellipses indicated that the error in ϵ is primarily a measure of the deviation in shape from an ellipse. We also measured the rotation of the ellipses with respect to each other by measuring the angles between the semimajor axes of the ellipses. The quantity $\Delta\theta$ is the maximum angle between the semimajor axes of the fitted ellipses.

To evaluate the precision of the contour tracing, 20 clusters representing a variety of morphological structures were traced two or more times. The agreement between the measures of ϵ was in general $\leq\pm0.02$; therefore, we confidently assumed that the systematic error associated with our procedure is $\leq\pm0.03$. The few contours with larger differences also had larger error bars on ϵ, and visual inspection revealed that these contours clearly depart from true ellipses. These departures appear to be the major source of the error in ϵ and not the contour tracing procedure. In our analysis of the fitted ellipses we excluded these measurements.

[2] https://automeris.io

4. Ellipticity measurements

4.1. Morphological parameters

We applied our tested procedure to extract ellipticity morphological parameters from the ICM X-ray density contours of the clusters listed in Tables A.1, A.2, and A.3. We investigated the use of some parameters to provide useful information about the dynamical state of clusters, based on their underlying elliptical X-ray morphology. As shown in the listing of Table A.4, four specific parameters extracted from the fitted ellipses were selected as possible indicators for cluster dynamical classification ($\Delta\epsilon$, ϵ max, $\Delta\theta$, ϵ profile). In particular, we considered the (ϵ profile) as the most basic first parameter to be used for a preliminary classification; it is the measured run of ellipticity outward from the cluster center. The other three, which are ellipticity (ϵ max) of the most flattened contour, the overall variation in ellipticity ($\Delta\epsilon$) measured for contours of each cluster, and the maximum rotation angle ($\Delta\theta$) of the fitted ellipses, may complement and support the cluster dynamical classification.

The ellipticity profile listed in the last column of Table A.4 describes how the ellipticity that we have extracted from the ICM contours of each galaxy cluster in our sample is varying as we move outward from the cluster center. This (ϵ profile) can be described in five different trends:

(1) ellipticity essentially constant, 13% of the total clusters ($\Delta\epsilon \leq 0.06$, given the maximum systematic error ±0.03 associated with our measuring procedure);

(2) ellipticity increasing monotonically outward from the cluster center, 22% of the total clusters;

(3) ellipticity increasing from the cluster center to a maximum and then decreasing outward (peaked), 16% of the total clusters;

(4) ellipticity decreasing monotonically from the cluster center, 42% of the total clusters;

(5) ellipticity decreasing from the cluster center and then increasing outward (dip), 7% of the total clusters.

The ($\Delta\epsilon$) parameter describes the change in flattening that occurs in the configuration of the hot gas inside clusters. The highest change ($\Delta\epsilon = 0.5$) is measured in non-relaxed clusters and the smallest value ($\Delta\epsilon = 0.03$) belongs to the relaxed clusters, with intermediate clusters in between. The parameter (ϵ max) shows a similar trend with (ϵ max) highest in non-relaxed clusters (ϵ max = 0.68) and smallest in relaxed clusters (ϵ max = 0.09). The rotation angle ($\Delta\theta$) of the fitted ellipses has less definite numbers for the two groups of clusters, with minimum ($\Delta\theta \sim 3°$) and maximum values ($\Delta\theta \sim 120°$) equally distributed between them. In the literature we found some comparison data for our ellipticity parameters of ICM density contours (see Sect. 5), but nothing equivalent to our ellipticity profiles.

4.2. Ellipticity profile data

Our plots of (ϵ profile) for ICM contours are illustrated in Figs. B.1, B.2, and B.3. Each figure refers to a group of clusters in our sample with a specific dynamical state classification: relaxed, non-relaxed, and intermediate. The projected radius in arcminutes of the contours has been converted to kiloparsec (upper scale of the figures) by using the cosmology calculator of Wright (2006) with $H_o = 69.6\,km\,s^{-1}\,Mpc^{-1}$, $\Omega_M = 0.286$, and $\Omega_\Lambda = 0.714$.

Table 1. Frequency of incidence for the classes of ellipticity profiles.

Clusters (1)	const. (2)	incr. (3)	peaked (4)	decr. (5)	dip (6)
Relaxed	33%	44%	14%	7%	2%
Non-Relaxed	···	4%	13%	79%	4%
Intermediate	···	13%	33%	27%	27%

Notes. (1) Dynamical state of sample clusters, (2) Ellipticity essentially constant, (3) Ellipticity increasing outward from the cluster center, (4) Ellipticity increasing and then decreasing outward (ϵ peaked), (5) Ellipticity decreasing outward, (6) Ellipticity decreasing and then increasing outward (ϵ dip).

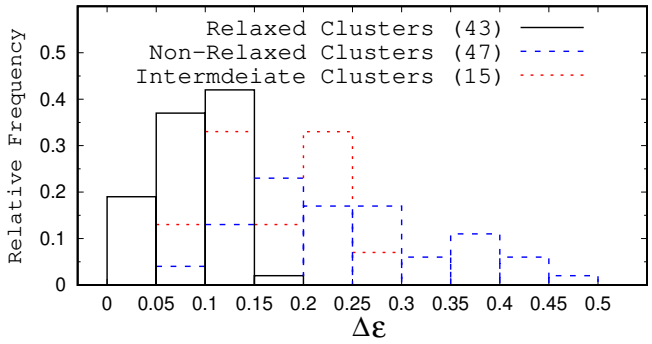

Fig. 3. Distribution of relative frequencies for the increment in ellipticity ($\Delta\epsilon$) between the least and the most flattened fitted ellipse to the ICM contours, for our three groups of clusters.

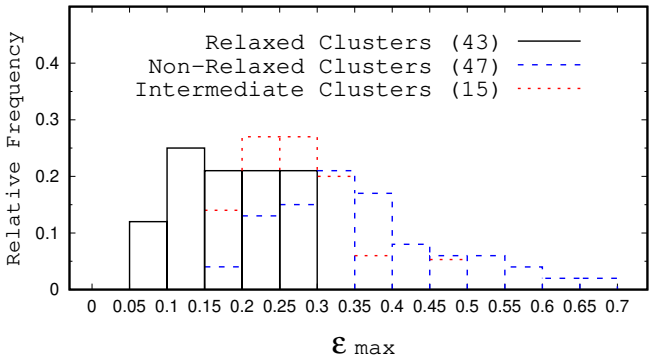

Fig. 4. Distribution of relative frequencies for the ellipticity (ϵ max) of the most flattened fitted ellipse to the ICM X-ray contours, for our three groups of clusters.

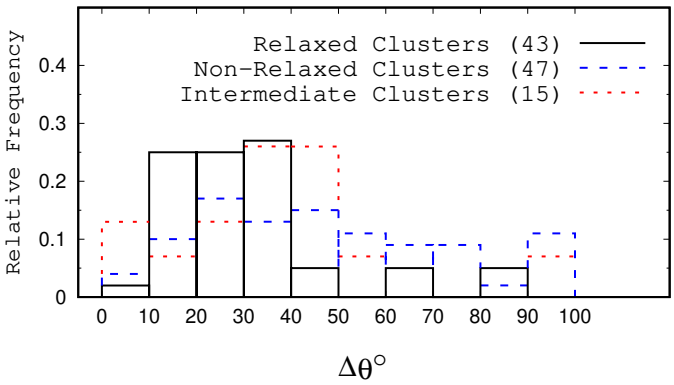

Fig. 5. Distribution of relative frequencies for the maximum rotation angle ($\Delta\theta$) in degrees, between the semimajor axes of the fitted ellipses, for our three groups of clusters.

The ellipticity profiles for the 43 relaxed clusters in Fig. B.1 present a concentration (44%) of increasing trends outward from the cluster center. Constant (ϵ profile) follows with 33% of the relaxed clusters. Then there is a smaller number of clusters with peaked (ϵ profile) (14%), and also with (ϵ profile) decreasing (7%) or (ϵ profile) with a dip (2%). For the 47 non-relaxed clusters in our sample, Fig. B.2 indicates a different general elliptical substructure. The majority concentrate on ellipticity profiles decreasing outward from the cluster center (79%), followed by 13% with peaked (ϵ profile), 4% with increasing (ϵ profile) or with a dip, and none with constant (ϵ profile). In Fig. B.3 we note that the 15 clusters of the intermediate group do not present a specific concentration of ellipticity profiles, although it is of some relevance that their ellipticity does not show a constant trend, as for the non-relaxed clusters. Based on this analysis, it appears that only galaxy clusters that are classified as dynamically relaxed present ICM density X-ray contours that are more symmetrical with no variation in ellipticity or at least with ellipticity very close to constant. Table 1 summarizes these results.

The clusters with a constant ellipticity profile have been classified by several authors, and by different parameters, as being in a dynamical relaxed state, as reported in Table A.1. Some of them, X-CLASS 21325 and X-CLASS 24004, have even been considered strongly relaxed (Parekh et al. 2015) or very relaxed, for example X-CLASS 23195 (Mantz et al. 2015). Other clusters, X-CLASS 1701 and X-CLASS 20679, have been described as having extremely regular X-ray morphologies (Govoni et al. 2009). As a result, the most extreme cases of dynamical state, both relaxed and non-relaxed, could be quickly identified by the simple morphological parameter (ϵ profile) of their intracluster hot gas: constant profile for relaxed clusters and far from constant for non-relaxed clusters.

4.3. Dynamical state separation

The plots of the ellipticity profiles for the ICM X-ray contours displayed in Figs. B.1, B.2, and B.3, show different ϵ trends for dynamically relaxed and non-relaxed clusters. The frequency of incidence for the morphology parameter (ϵ profile), as summarized in Table 1, highlights a separation between dynamical relaxation and non-relaxation, based on the increase or decrease of X-ray contour ellipticity, measured outward from the cluster center. Relaxed clusters have a tendency to develop a more elliptical substructure farther from the core (ϵ profile increasing), while the non-relaxed clusters are more elliptical closer to the center (ϵ profile decreasing).

An equivalent separation derived from two other morphology parameters is emphasized by the distributions of relative frequencies for the total variation in ellipticity ($\Delta\epsilon$) and for the maximum ellipticity (ϵ max) value, as shown by the histograms in Fig. 3 and in Fig. 4. The ($\Delta\epsilon$) parameter separates the relaxed clusters from the non-relaxed clusters around a 0.15 value ($\Delta\epsilon \leq 0.15$ for the relaxed), leaving a few non-relaxed clusters in the overlap area with the relaxed (8 out of 47). The parameter (ϵ max) separates the relaxed clusters from most of the non-relaxed clusters around the value 0.3, with (ϵ max) ≤ 0.3 for the relaxed. In this case there are more non-relaxed clusters (15 out of 47) in the overlap area with the relaxed clusters. Intermediate clusters fill both areas, as expected according to their intermediate state of evolution, in some cases closer to becoming dynamically relaxed, in other cases still in a disturbed dynamical

state. Figure 5 shows that the ($\Delta\theta$) parameter is less effective than the other two in separating relaxed from non-relaxed clusters. There is only a minor shifting of ($\Delta\theta$) toward smaller values for clusters classified as dynamically relaxed. The significant overlap of the three groups suggests a complexity of dynamical processes related to the hydrostatic equilibrium within clusters, with the creation of different levels of turbulence in the ICM and twisting of its density contours, somehow independent from the cluster dynamical state.

5. Comparison with ellipticity data from other ICM contours

In our analysis of the highlighted elliptical configuration within galaxy clusters, we have found that the dynamical state of the clusters in our sample seems to be adequately represented by the values of specific morphology ellipticity parameters for the ICM X-ray density contours that we utilized. To validate the results of our procedure, we searched for X-ray contours computed by other studies for galaxy clusters also belonging to our sample. We compared 23 clusters in common by applying to them our procedure for fitting ellipses to these different contours. We computed their total variation in ellipticity ($\Delta\epsilon$), their maximum and mean ellipticity (ϵ max) and (ϵ mean), and their outward ellipticity (ϵ profile). We had to introduce a new parameter (ϵ mean) since it seems to be the most used in the literature, which also allowed a direct comparison with those data (Table A.5).

Table A.5 shows a good agreement for the selected morphological parameters, within the systematic error of our measurements, between the values obtained from the contours that we used and the values that we obtained from the contours provided by other authors from different X-ray observations. Even the ϵ profiles are in general agreement, with the exception of four relaxed clusters. This overall correspondence supports the assumption that our adopted elliptical metrics for dynamical cluster classification, could have a general application to a variety of ICM density contours.

In the case of X-CLASS 1701, 21325, and 22878, the difference in the profile classification from "constant" versus "increasing" does not remove the clusters from being identified as dynamically relaxed in our adopted classification system. The fourth cluster, X-CLASS 24615, with its constant (ϵ profile) versus our decreasing profile, more typical in our classification for non-relaxed clusters, points to the importance of carefully evaluating any exception. This can lead to a better understanding of the multidimensional complexity affecting the cluster dynamical state. A recent study (Haggar et al. 2024) has shown that there are different classes of dynamically relaxed clusters with different properties, connected with the formation state of the clusters, their local environment and merger history. However, even amid this complexity, it is still meaningful to develop a dynamical classification as a starting point for evaluating the state of relaxation of galaxy clusters.

6. Results and discussion

The data presented in the previous sections provide a good starting point for considering the ellipticity parameters ($\Delta\epsilon$, ϵ max, ϵ profile) that we used to describe the configuration of ICM contours, as basic preliminary morphology indicators for galaxy clusters. Because of the correspondence shown in Table A.5, these three parameters should indicate the potential dynamical state independently of the data used and the method employed to produce the contours of the X-ray cluster images.

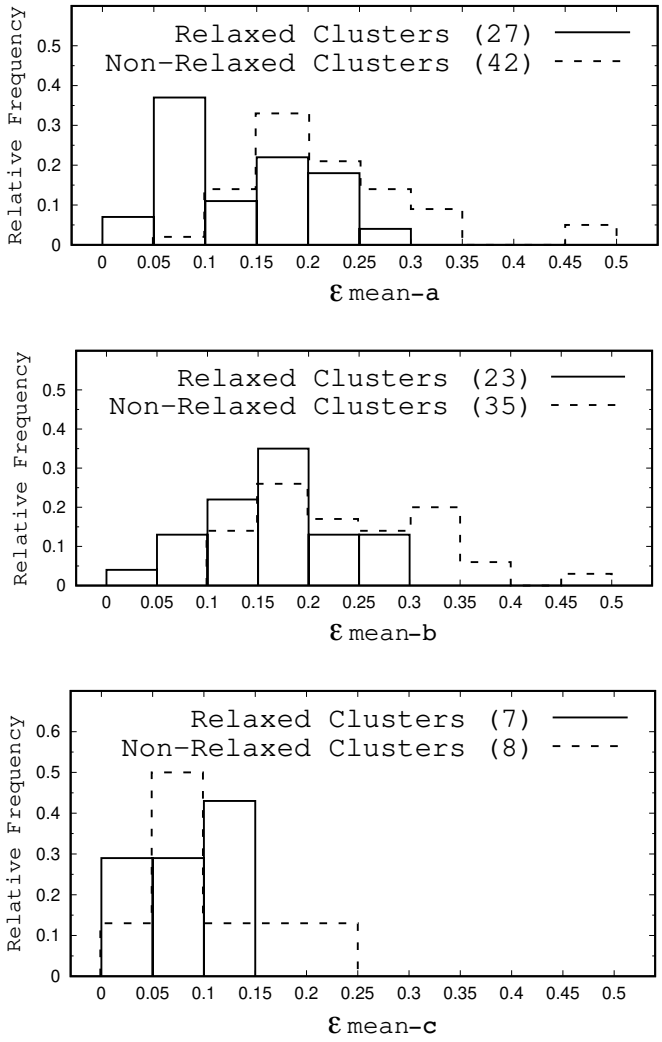

Fig. 6. Distribution of relative frequencies for the mean ellipticity (ϵ mean) measured by different authors as listed in Table A.6, (ϵ mean-a) from our metrics; (ϵ mean-b) from isophotes measured by Mantz et al. (2015); (ϵ mean-c) from X-ray flux measured by Parekh et al. (2015).

This assumption about X-ray contour compatibility is also supported by comparing our mean ellipticity measurements with those provided by other authors for 69 clusters in common. The data listed in Table A.6 show a common trend of values for our measurements of mean ICM ellipticity (ϵ mean) and those provided by two other authors from different sets of contours. More importantly, all three provide lower values for relaxed clusters. The similar trend for the distribution of relative frequencies between the (ϵ mean) measured by our metrics and the (ϵ mean) measured by other methods, may be considered a validation of our results. The overall trend of the different measures is more valuable than the specific numbers, which are subject to systematic errors.

However the data in Table A.6, when plotted in the histograms of Fig. 6, do not support considering (ϵ mean) as a reliable indicator for cluster dynamical state. The non-relaxed group of galaxy clusters presents only a minor shifting to higher values of (ϵ mean), leaving an overlap for most of the clusters, both relaxed and non-relaxed. This result confirms a previous finding by Parekh et al. (2015), that the mean ellipticity measured for the X-ray flux in cluster images is not an effective parameter

for separating relaxed from non-relaxed clusters. Mantz et al. (2015) also found that although the lowest mean ellipticity of employed isophotes are in relaxed clusters and the highest are in non-relaxed, the two distributions overlap significantly. A simple interpretation could be that the dynamical state of clusters does not seem to affect their ellipsoid shape directly.

We had a similar outcome of cluster overlapping for the frequency distribution of the twisting of ICM contours measured by ($\Delta\theta$) (Fig. 5). Again, a simple interpretation could be that the underlying elliptical structure of clusters is not much affected by the turbulence in the ICM gas.

A different perspective is offered by the measurements obtained with other two ellipticity parameters that we selected as promising indicators for cluster dynamic classification: ($\Delta\epsilon$) and (ϵ max). The distributions of their relative frequencies, as illustrated in Figs. 3 and 4, emphasize a clear enough separation between relaxed and non-relaxed clusters around a 0.15 value for ($\Delta\epsilon$) and a 0.3 value for (ϵ max). The ellipticity profile provides an even more significant separation between relaxed and non-relaxed clusters, as illustrated in Figs. B.1 and B.2 and discussed in Sect. 4.3.

7. Conclusions

By using a combination of three morphology parameters, (ϵ profile), ($\Delta\epsilon$), (ϵ max), extracted from ellipses fitted to the ICM X-ray density contours in our sample of 105 clusters, we investigated galaxy clusters already dynamically classified. With these metrics, we were able to separate them into two groups corresponding to the anticipated dynamical state, with some expected overlapping, given the complex dynamics of clusters. The main points that have emerged from this study are the following:

1. The underlying elliptical configuration of the intracluster medium (ICM) presents five different ellipticity trends outward from the cluster center: (ϵ profile) constant, increasing, decreasing, with a peak, and with a dip.
2. There is a significant correlation between the dynamical state of clusters and their ICM ellipticity profile:
   (a) A majority of relaxed clusters present an ellipticity profile constant or increasing outward (77%), with a small percentage of the other trends.
   (b) A majority of non-relaxed clusters present a decreasing ellipticity profile (79%), also with a small percentage of the other trends, but no ϵ constant.
3. There is a significant correlation between the dynamical state of clusters and their ICM total variation in ellipticity ($\Delta\epsilon$):
   (a) The majority of relaxed clusters (98%) present a ($\Delta\epsilon$) $\leq$ 0.15.
   (b) Most non-relaxed clusters (83%) present a ($\Delta\epsilon$) $>$ 0.15.
4. There is a good correlation between the dynamical state of clusters and their ICM maximum ellipticity (ϵ max).
   (a) 100% of relaxed clusters have (ϵ max) $\leq$ 0.3.
   (b) 70% of non-relaxed clusters have (ϵ max) $>$ 0.3.

On the basis of the results from this study, we propose the following strategy for a quick initial, preliminary assessment of the dynamical state of a galaxy cluster, which deserves a more in depth study. First search for ICM X-ray contours provided by the archives of X-ray Observatories. Then develop a procedure to fit ellipses to the contours and extract the ellipticity parameters used in this study, or any others more appropriate for that specific analysis. Last, create a scale of values for dynamical state separation.

In our study, the preliminary scale of values would be the following:

1. Dynamically relaxed clusters: (ϵ profile) constant (high probability of being relaxed) or increasing outward from the center, with ($\Delta\epsilon$) $\leq$ 0.15 and (ϵ max) $\leq$ 0.3 (probably relaxed or close to being relaxed). The other ellipticity trends and numerical values are ambiguous (see Table 1 and Figs. 4 and 5), confirming the multidimensional complexity of cluster dynamical states.
2. Dynamically non-relaxed clusters: (ϵ profile) decreasing outward from the center, with ($\Delta\epsilon$) $>$ 0.15 and (ϵ max) $>$ 0.3.
3. Dynamically intermediate clusters: Values overlapping the other two groups, difficult classification just on ellipticity.

As a follow up to this study, we plan to apply our tested procedure for a preliminary dynamical classification of galaxy clusters spectroscopically confirmed in the X-CLASS Survey Catalogue that were not in our selected subsample, up to 500 new objects. We also plan to study a comparable number of clusters from more recent catalogs. The aim is to provide a larger homogeneous sample of morphologically classified clusters, less subject to selection effects.

References

Biviano, A. 2000, in Constructing the Universe with Clusters of Galaxies, eds. F. Durret, & D. Gerbal, 1
Böhringer, H., Chon, G., & Fukugita, M. 2017, A&A, 608, A65
Casas, M. C., Putnam, K., Mantz, A. B., Allen, S. W., & Somboonpanyakul, T. 2024, ApJ, 967, 14
Cerini, G., Cappelluti, N., & Natarajan, P. 2023, ApJ, 945, 152
Coe, D., Benítez, N., Broadhurst, T., & Moustakas, L. A. 2010, ApJ, 723, 1678
De Young, D. S. 1978, ApJ, 223, 47
di Tullio, G. 1978, A&A, 62, L17
di Tullio, G. A. 1979, A&AS, 37, 591
Ebeling, H., Barrett, E., Donovan, D., et al. 2007, ApJ, 661, L33
Ebeling, H., Richard, J., Beauchesne, B., et al. 2025, MNRAS, 537, 2662
Flin, P. 1984, in Clusters and Groups of Galaxies, eds. F. Mardirossian, G. Giuricin, & M. Mezzetti, Astrophys. Space Sci. Lib., 111, 163
Govoni, F., Murgia, M., Markevitch, M., et al. 2009, A&A, 499, 371
Gunn, J. E., & Gott, J. R., III. 1972, ApJ, 176, 1
Haggar, R., De Luca, F., De Petris, M., et al. 2024, MNRAS, 532, 1031
Harvey, D., Tam, S.-I., Jauzac, M., Massey, R., & Rhodes, J. 2019, ArXiv e-prints [arXiv:1911.06333]
Heinrich, A., Zhuravleva, I., Zhang, C., et al. 2024, MNRAS, 528, 7274
Huang, H.-J., Mandelbaum, R., Freeman, P. E., et al. 2016, MNRAS, 463, 222
Hudson, D. S., Mittal, R., Reiprich, T. H., et al. 2010, A&A, 513, A37
Koulouridis, E., Clerc, N., Sadibekova, T., et al. 2021, A&A, 652, A12
Łokas, E. L. 2023, A&A, 673, A131
Mantz, A. B., Allen, S. W., Morris, R. G., et al. 2015, MNRAS, 449, 199
Mantz, A. B., Allen, S. W., Morris, R. G., et al. 2017, MNRAS, 472, 2877
Mantz, A. B., Morris, R. G., Allen, S. W., et al. 2022, MNRAS, 510, 131
McDonald, M., Allen, S. W., Hlavacek-Larrondo, J., et al. 2019, ApJ, 870, 85
Parekh, V., van der Heyden, K., Ferrari, C., Angus, G., & Holwerda, B. 2015, A&A, 575, A127
Pratt, G. W., Arnaud, M., Biviano, A., et al. 2019, Space Sci. Rev., 215, 25
Sarazin, C. L. 1986, Rev. Mod. Phys., 58, 1
Schmidt, R. W., & Allen, S. W. 2007, MNRAS, 379, 209
Sereno, M., Umetsu, K., Ettori, S., et al. 2018, ApJ, 860, L4
Shankar, S., & Khatri, R. 2021, MNRAS, 503, 2791
Tchernin, C., Lau, E. T., Stapelberg, S., Hug, D., & Bartelmann, M. 2020, A&A, 644, A126
Tempel, E., Tuvikene, T., Kipper, R., & Libeskind, N. I. 2017, A&A, 602, A100
Véliz Astudillo, S., Carrasco, E. R., Nilo Castellón, J. L., Zenteno, A., & Cuevas, H. 2025, A&A, 693, A106
Wright, E. L. 2006, PASP, 118, 1711
Yuan, Z. S., Han, J. L., & Wen, Z. L. 2022, MNRAS, 513, 3013
Zhang, B., Cui, W., Wang, Y., Dave, R., & De Petris, M. 2022, MNRAS, 516, 26

Appendix A: Tables

Table A.1. List of the dynamically relaxed clusters analyzed in this work.

X-CLASS (1)	Other ID (2)	RA (deg.)(3)	Dec (deg.)(4)	z (5)	References (6)
174	Abell 478	63.35720	10.46370	0.088	8, 10, 11
707	···	255.34500	64.23720	0.452	10
926	Abell S84	12.34320	-29.52050	0.109	13
1019	···	250.42700	39.12580	0.592	10
1363	eMACS J2327.4	351.86801	-2.07840	0.700	3
1637	Abell 963	154.26401	39.04890	0.206	11, 14
1701	Abell 1413	178.82800	23.40150	0.141	4, 6, 11, 14
1767	···	213.79700	36.20010	1.027	8
2466	Abell 611	120.23400	36.05480	0.286	11
2497	···	233.22501	30.34930	0.362	6
2772	···	40.64860	-21.54050	0.314	8, 11
2775	Abell 586	113.08500	31.63250	0.171	6
2903	Abell 3343	81.45450	-47.24940	0.191	13
3097	Abell 3112	49.48940	-44.23810	0.074	10
3134	···	30.42890	-2.19660	0.196	13
3153	···	337.43900	-27.92380	0.322	8, 11
3190	Abell 2697	0.80200	-6.09280	0.234	13
3337	···	325.06400	-23.66050	0.315	6, 8
3414	···	168.96600	1.49950	0.352	8, 11
3417	Abell 2261	260.61200	32.13280	0.224	5
3490	Abell 133	15.67290	-21.88150	0.057	6, 8, 10, 14
20679	Abell 1068	160.18401	39.95120	0.136	4, 8
20682	···	138.44000	40.94030	0.443	8
20710	Abell 2667	357.91299	-26.08340	0.233	5, 8
20725	Abell 3827	330.47101	-59.94550	0.100	13
20981	···	179.96700	55.53460	0.080	8
21325	Abell 2204	248.19501	5.57550	0.152	8, 10, 11, 14
21391	Zwicky 2089	135.15401	20.89440	0.235	8
21601	···	146.79700	76.38620	0.354	6, 8, 11
22878	Abell 383	42.01410	-3.52830	0.190	5, 8, 11
22908	Abell 1689	197.87199	-1.34180	0.183	1
22909	···	322.41501	0.08740	0.233	8, 11
23195	Abell 1835	210.25800	2.87800	0.251	4, 5, 8, 11, 14
23225	Abell 901/902	148.99001	-9.98450	0.162	11
23388	···	303.71500	-24.50600	0.161	8
23788	Abell 2811	10.52970	-28.53760	0.107	13
23843	···	260.04099	26.62510	0.161	8
23933	Abell 780	139.52499	-12.09570	0.054	6, 8
24004	Abell 2029	227.73399	5.74490	0.075	4, 8, 10, 11
24008	MACS J0744.8	116.21600	39.45600	0.697	2, 5, 11
24641	···	260.07001	35.60640	0.390	5, 8
24645	MACS J1423.8	215.95100	24.07940	0.542	2, 6, 8, 11
24690	···	356.18301	-42.71960	0.594	6, 8, 9

Notes. (1) X-CLASS cluster ID number, (2) Other ID, (3) Right ascension, (4) Declination, (5) Redshift (spectroscopic from the X-CLASS catalog), (6) References for the classified dynamical state of each cluster that we used to calibrate our classifications.

References. 1-Coe et al. (2010), 2-Ebeling et al. (2007), 3-Ebeling et al. (2025), 4-Govoni et al. (2009), 5-Harvey et al. (2019), 6-Heinrich et al. (2024), 7-Łokas (2023), 8-Mantz et al. (2015), 9-McDonald et al. (2019), 10-Parekh et al. (2015), 11-Schmidt & Allen (2007), 12-Tempel et al. (2017), 13-Véliz Astudillo et al. (2025), 14-Yuan et al. (2022), 15-Casas et al. (2024)

Table A.2. List of the dynamically non-relaxed clusters analyzed in this work.

X-CLASS (1)	Other ID (2)	RA (deg.)(3)	Dec (deg.)(4)	z (5)	References (6)
96	Abell 68	9.27650	9.15830	0.252	8, 14
97	Abell 209	22.97030	-13.61470	0.209	8, 14
243	Abell 496	68.41180	-13.26640	0.033	8, 10
292	···	85.02940	-40.83890	0.037	10
428	Abell 3558	201.99001	-31.49760	0.048	10
458	MACS J0018.5	4.63800	16.43560	0.546	2
470	···	208.57201	-2.36560	0.548	10
706	···	170.03000	43.30070	0.609	10
759	Abell 2218A	248.97000	66.20890	0.176	8
836	Abell 2034	227.54500	33.51260	0.113	8, 15
1338	Abell 907	149.59200	-11.06390	0.166	8
1846	Abell 3888	338.61200	-37.73620	0.155	14
1927	MACS J0454.1	73.54890	-3.01380	0.540	2
2041	···	14.01260	-37.54680	0.165	8
2064	Abell 3395E	96.89990	-54.45210	0.051	10
2086	Hercules	252.78400	4.99270	0.154	8
2101	···	51.97450	2.56290	0.030	8
2152	Abell 1201	168.22600	13.43560	0.168	8, 14
2202	···	340.84100	-9.59690	0.447	8
2320	Abell 754	137.34100	-9.67690	0.054	7, 10
2449	···	354.35101	-59.70470	0.778	8
2450	···	89.93080	-52.82760	0.608	8
2467	Abell 697	130.73700	36.36470	0.281	8
2571	Abell S295	41.37200	-53.03820	0.301	6
2842	Abell 2420	332.58200	-12.17510	0.085	8
2843	Abell 2426	333.63199	-10.37200	0.103	8
2951	MACS J1149.5	177.39700	22.40160	0.544	2, 8
2955	MACS J2214.9	333.73999	-14.00310	0.503	2, 8
2976	MACS J2129.4	322.35599	-7.69050	0.587	2, 8
3114	Abell 521	73.53780	-10.24030	0.246	8, 14
3137	Zwicky 3146	155.91600	4.18630	0.291	8
3150	···	99.69890	-53.97350	0.226	8
3249	···	181.63200	-7.74140	0.068	8
3297	MACS J0717.5	109.38000	37.75820	0.549	2, 6, 8
20188	Abell 773	139.47099	51.72390	0.219	6, 8
20463	Abell 1914	216.50301	37.82620	0.167	6, 8, 12
22639	···	72.48390	-44.67210	0.149	8
22663	eMACS1508.1	227.08000	57.91530	0.539	3
22988	Abell 1775	205.45200	26.37280	0.076	8
23095	Bullet	104.62600	-55.94360	0.296	6, 7, 8
23375	Abell 3364	86.90890	-31.87080	0.148	8
24547	Abell 2645	355.32001	-9.02450	0.251	8
24615	Abell 2163	243.94200	-6.14730	0.200	8, 10, 11
24630	···	239.59000	-14.16570	0.097	8
24787	···	316.51801	-58.74210	1.129	8
24790	···	355.30099	-51.32960	1.003	8
24797	···	326.64499	-46.54880	0.928	8

Notes. and References: see Table A.1

Table A.3. List of the dynamically intermediate clusters analyzed in this work.

X-CLASS (1)	Other ID (2)	RA (deg.)(3)	Dec (deg.)(4)	z (5)	References (6)
82	Abell 3038	39.49290	-52.39370	0.136	13
201	Abell 2390	328.40601	17.69610	0.230	6
1266	Abell 2052	229.18600	7.02230	0.035	6
1683	Abell 1795	207.22099	26.58930	0.062	6
2190	···	181.55000	-8.80010	0.438	6
2234	Abell S1063	342.18900	-44.52820	0.348	6, 13
2464	Abell 2219	250.08701	46.71420	0.226	6
3496	Abell 85	10.45870	-9.30330	0.055	6
20004	Abell 2199	247.15800	39.55030	0.030	6
20538	···	206.87700	-11.75190	0.450	6
22419	Abell S579	94.13530	-39.80120	0.152	13
22991	Zwicky 7160	224.31200	22.34120	0.255	6
23220	···	337.13599	20.61900	0.412	6
23229	Abell 2626	354.12799	21.14660	0.055	6
24550	···	292.95599	-26.57530	0.358	6

Notes. and References: see Table A.1.

Table A.4. Ellipticity measurements for the galaxy clusters analyzed in this work.

X-CLASS (1)	Other ID (2)	Dynamical State (3)	$\Delta\epsilon$ (4)	ϵ max (5)	$\Delta\theta^0$ (6)	ϵ profile (7)
82	Abell 3038	Intermediate	0.22	0.35	38	Peaked
96	Abell 68	Non-Relaxed	0.16	0.35	20	Decreasing
97	Abell 209	Non-Relaxed	0.20	0.41	7	Decreasing
174	Abell 478	Relaxed	0.12	0.29	16	Peaked
201	Abell 2390	Intermediate	0.16	0.34	10	Peaked
243	Abell 496	Non-Relaxed	0.17	0.25	85	Increasing
292	···	Non-Relaxed	0.26	0.46	28	Decreasing
428	Abell 3558	Non-Relaxed	0.18	0.35	26	Peaked
458	MACS J0018.5	Non-Relaxed	0.10	0.22	63	Decreasing
470	···	Non-Relaxed	0.29	0.38	35	Decreasing
706	···	Non-Relaxed	0.28	0.33	111	Decreasing
707	···	Relaxed	0.12	0.24	34	Peaked
759	Abell 2218A	Non-Relaxed	0.22	0.31	74	Decreasing
836	Abell 2034	Non-Relaxed	0.19	0.26	95	Peaked
926	Abell S84	Relaxed	0.06	0.21	103	Constant
1019	···	Relaxed	0.11	0.26	24	Increasing
1266	Abell 2052	Intermediate	0.15	0.23	41	Increasing
1338	Abell 907	Non-Relaxed	0.14	0.29	25	Dip
1363	eMACS J2327.4	Relaxed	0.12	0.21	26	Peaked
1637	Abell 963	Relaxed	0.09	0.15	63	Peaked
1683	Abell 1795	Intermediate	0.14	0.27	31	Dip
1701	Abell 1413	Relaxed	0.04	0.30	11	Constant
1767	···	Relaxed	0.05	0.10	89	Constant
1846	Abell 3888	Non-Relaxed	0.08	0.29	64	Decreasing
1927	MACS J0454.1	Non-Relaxed	0.19	0.27	56	Decreasing
2041	···	Non-Relaxed	0.28	0.34	31	Decreasing
2064	Abell 3395E	Non-Relaxed	0.41	0.68	3	Decreasing
2086	Hercules	Non-Relaxed	0.26	0.35	48	Decreasing
2101	···	Non-Relaxed	0.36	0.40	54	Decreasing
2152	Abell 1201	Non-Relaxed	0.28	0.52	21	Peaked
2190	···	Intermediate	0.22	0.25	40	Decreasing
2202	···	Non-Relaxed	0.38	0.53	36	Decreasing
2234	Abell S1063	Intermediate	0.23	0.30	32	Decreasing
2320	Abell 754	Non-Relaxed	0.30	0.64	22	Decreasing
2449	···	Non-Relaxed	0.21	0.25	68	Decreasing
2450	···	Non-Relaxed	0.21	0.47	19	Decreasing
2464	Abell 2219	Intermediate	0.22	0.38	18	Decreasing
2466	Abell 611	Relaxed	0.10	0.14	31	Increasing
2467	Abell 697	Non-Relaxed	0.16	0.28	42	Decreasing
2497	···	Relaxed	0.14	0.24	23	Increasing
2571	Abell S295	Non-Relaxed	0.37	0.39	33	Decreasing
2772	···	Relaxed	0.09	0.14	39	Increasing
2775	Abell 586	Relaxed	0.12	0.14	24	Decreasing
2842	Abell 2420	Non-Relaxed	0.37	0.54	43	Decreasing
2843	Abell 2426	Non-Relaxed	0.12	0.21	27	Decreasing
2903	Abell 3343	Relaxed	0.12	0.26	17	Peaked
2951	MACS J1149.5	Non-Relaxed	0.35	0.41	60	Decreasing
2955	MACS J2214.9	Non-Relaxed	0.23	0.32	44	Decreasing
2976	MACS J2129.4	Non-Relaxed	0.20	0.21	80	Decreasing
3097	Abell 3112	Relaxed	0.09	0.26	16	Increasing
3114	Abell 521	Non-Relaxed	0.45	0.59	53	Peaked
3134	···	Relaxed	0.14	0.17	18	Increasing
3137	Zwicky 3146	Non-Relaxed	0.15	0.20	51	Peaked
3150	···	Non-Relaxed	0.15	0.36	37	Decreasing
3153	···	Relaxed	0.11	0.19	18	Increasing
3190	Abell 2697	Relaxed	0.09	0.23	37	Increasing

Table A.4. continued.

X-CLASS (1)	Other ID (2)	Dynamical State (3)	$\Delta\epsilon$ (4)	ϵ max (5)	$\Delta\theta^0$ (6)	ϵ profile (7)
3249	···	Non-Relaxed	0.16	0.26	49	Decreasing
3297	MACS J0717.5	Non-Relaxed	0.17	0.38	22	Decreasing
3337	···	Relaxed	0.06	0.10	12	Constant
3414	···	Relaxed	0.04	0.23	25	Constant
3417	Abell 2261	Relaxed	0.09	0.12	30	Increasing
3490	Abell 133	Relaxed	0.08	0.20	66	Increasing
3496	Abell 85	Intermediate	0.10	0.18	21	Dip
20004	Abell 2199	Intermediate	0.14	0.23	45	Dip
20188	Abell 773	Non-Relaxed	0.18	0.34	21	Decreasing
20463	Abell 1914	Non-Relaxed	0.50	0.57	47	Decreasing
20538	···	Intermediate	0.15	0.29	41	Dip
20679	Abell 1068	Relaxed	0.03	0.28	25	Constant
20682	···	Relaxed	0.03	0.12	40	Constant
20710	Abell 2667	Relaxed	0.15	0.24	36	Decreasing
20725	Abell 3827	Relaxed	0.06	0.17	123	Constant
20981	···	Relaxed	0.09	0.11	31	Increasing
21325	Abell 2204	Relaxed	0.06	0.10	81	Constant
21391	Zwicky 2089	Relaxed	0.15	0.30	17	Increasing
21601	···	Relaxed	0.15	0.28	31	Increasing
22419	Abell S579	Intermediate	0.25	0.47	9	Decreasing
22639	···	Non-Relaxed	0.43	0.44	80	Decreasing
22878	Abell 383	Relaxed	0.12	0.13	11	Increasing
22908	Abell 1689	Relaxed	0.13	0.16	35	Increasing
22909	···	Relaxed	0.06	0.24	3	Constant
22988	Abell 1775	Non-Relaxed	0.25	0.29	109	Peaked
22991	Zwicky 7160	Intermediate	0.16	0.22	29	Increasing
23095	Bullet	Non-Relaxed	0.25	0.37	66	Decreasing
23195	Abell 1835	Relaxed	0.06	0.12	27	Constant
23220	···	Intermediate	0.08	0.28	102	Peaked
23225	Abell 901/902	Relaxed	0.03	0.14	35	Constant
23229	Abell 2626	Intermediate	0.11	0.20	54	Peaked
23375	Abell 3364	Non-Relaxed	0.14	0.19	75	Dip
23388	···	Relaxed	0.17	0.18	101	Increasing
23788	Abell 2811	Relaxed	0.12	0.28	22	Decreasing
23843	···	Relaxed	0.11	0.15	43	Increasing
23933	Abell 780	Relaxed	0.13	0.17	45	Peaked
24004	Abell 2029	Relaxed	0.04	0.24	13	Constant
24008	MACS J0744.8	Relaxed	0.07	0.09	···	Dip
24547	Abell 2645	Non-Relaxed	0.32	0.42	18	Decreasing
24550	···	Intermediate	0.30	0.33	45	Peaked
24615	Abell 2163	Non-Relaxed	0.21	0.37	13	Decreasing
24630	···	Non-Relaxed	0.11	0.21	32	Decreasing
24641	···	Relaxed	0.12	0.19	15	Increasing
24645	MACS J1423.8	Relaxed	0.10	0.16	37	Increasing
24690	···	Relaxed	0.05	0.09	30	Constant
24787	···	Non-Relaxed	0.24	0.34	14	Decreasing
24790	···	Non-Relaxed	0.28	0.35	102	Increasing
24797	···	Non-Relaxed	0.33	0.36	96	Decreasing

Notes. (1) X-CLASS cluster ID number; (2) Other ID; (3) Dynamical state classified by different authors (see Tables 1, 2, and 3 for references); (4) Our measured total variation in ellipticity, ($\Delta\epsilon$), of the fitted ellipses to the ICM X-ray contours; (5) Our measured maximum ellipticity, (ϵ max); (6) Maximum angle, ($\Delta\theta$) in deg., between the semimajor axes of the fitted ellipses; (7) Our measured run of ellipticity outward from the center of the cluster, (ϵ profile).

Table A.5. Comparison of our ICM ellipticity morphological parameters applied to x-ray contours published by other authors, for clusters in common with our sample.

Name (1)	$\Delta\epsilon$ (2)	ϵ max (3)	ϵ mean (4)	ϵ profile (5)	Dynamical State (6)	References (7)
X-CLASS 96	0.16	0.35	0.27	Decreasing	Non-Relaxed	This work
Abell 68	0.19	0.35	0.28	Decreasing	Non-Relaxed	Yuan et al. (2022)
X-CLASS 97	0.20	0.41	0.32	Decreasing	Non-Relaxed	This work
Abell 209	0.17	0.32	0.24	Decreasing	Non-Relaxed	Yuan et al. (2022)
X-CLASS 458	0.10	0.22	0.17	Decreasing	Non-Relaxed	This work
eMACS J0018.5	0.18	0.22	0.17	Decreasing	Non-Relaxed	Ebeling et al. (2025)
X-CLASS 1363	0.12	0.21	0.15	Peaked	Relaxed	This work
eMACS J2327.4	0.07	0.27	0.23	Peaked	Relaxed	Ebeling et al. (2025)
X-CLASS 1637	0.09	0.15	0.11	Peaked	Relaxed	This work
Abell 963	0.11	0.13	0.09	Peaked	Relaxed	Yuan et al. (2022)
X-CLASS 1701	0.04	0.30	0.28	Constant	Relaxed	This work
Abell 1413	0.14	0.40	0.33	Increasing	Relaxed	Yuan et al. (2022)
X-CLASS 1846	0.08	0.29	0.25	Decreasing	Non-Relaxed	This work
Abell 3888	0.10	0.31	0.27	Decreasing	Non-Relaxed	Yuan et al. (2022)
X-CLASS 1927	0.19	0.27	0.20	Decreasing	Non-Relaxed	This work
eMACS J0454.1	0.19	0.38	0.28	Decreasing	Non-Relaxed	Ebeling et al. (2025)
X-CLASS 2152	0.28	0.52	0.35	Peaked	Non-Relaxed	This work
Abell 1201	0.39	0.55	0.33	Peaked	Non-Relaxed	Yuan et al. (2022)
X-CLASS 2951	0.35	0.41	0.23	Decreasing	Non-Relaxed	This work
eMACS J1149.5	0.40	0.45	0.31	Decreasing	Non-Relaxed	Ebeling et al. (2025)
X-CLASS 2955	0.23	0.32	0.18	Decreasing	Non-Relaxed	This work
eMACS J2214.9	0.20	0.36	0.29	Decreasing	Non-Relaxed	Ebeling et al. (2025)
X-CLASS 2976	0.20	0.21	0.06	Decreasing	Non-Relaxed	This work
eMACS 2129.4	0.31	0.33	0.14	Decreasing	Non-Relaxed	Ebeling et al. (2025)
X-CLASS 3114	0.45	0.59	0.28	Peaked	Non-Relaxed	This work
Abell 521	0.52	0.65	0.31	Peaked	Non-Relaxed	Yuan et al. (2022)
X-CLASS 3297	0.17	0.38	0.31	Decreasing	Non-Relaxed	This work
eMACS J0717.5	0.23	0.41	0.28	Decreasing	Non-Relaxed	Ebeling et al. (2025)
X-CLASS 3490	0.08	0.20	0.17	Increasing	Relaxed	This work
Abell 133	0.09	0.15	0.11	Increasing	Relaxed	Yuan et al. (2022)
X-CLASS 20073	0.33	0.42	0.28	Decreasing	Non-Relaxed	This work
Abell 2744	0.50	0.63	0.42	Decreasing	Non-Relaxed	Cerini et al. (2023)
X-CLASS 21325	0.06	0.10	0.08	Constant	Relaxed	This work
Abell 2204	0.08	0.19	0.17	Increasing	Relaxed	Mantz et al. (2015)
Abell 2204	0.09	0.14	0.08	Increasing	Relaxed	Yuan et al. (2022)
X-CLASS 22663	0.39	0.49	0.28	Decreasing	Non-Relaxed	This work
eMACS J1508.1	0.25	0.53	0.40	Decreasing	Non-Relaxed	Ebeling et al. (2025)
X-CLASS 22878	0.12	0.13	0.07	Increasing	Relaxed	This work
Abell 383	0.04	0.07	0.05	Constant	Relaxed	Cerini et al. (2023)
X-CLASS 23195	0.06	0.12	0.09	Constant	Relaxed	This work
Abell 1835	0.02	0.14	0.13	Constant	Relaxed	Mantz et al. (2015)
Abell 1835	0.03	0.11	0.09	Constant	Relaxed	Yuan et al. (2022)
X-CLASS 24008	0.07	0.09	0.06	Dip	Relaxed	This work
eMACS J0744.8	0.10	0.14	0.10	Dip	Relaxed	Ebeling et al. (2025)
X-CLASS 24615	0.21	0.37	0.25	Decreasing	Non-Relaxed	This work
Abell 2163	0.06	0.27	0.24	Constant	Non-Relaxed	Mantz et al. (2015)
X-CLASS 24645	0.10	0.16	0.10	Increasing	Relaxed	This work
eMACS J1423.8	0.08	0.22	0.17	Increasing	Relaxed	Ebeling et al. (2025)

Notes. (1) X-CLASS cluster ID number with below the ID used by the other author, (2) our measured total variation in ellipticity, ($\Delta\epsilon$), of the fitted ellipses to the ICM x-ray contours that are provided by the X-CLASS catalog, with below our measures for the contours published by another author, (3) our measured (ϵ max) for both set of contours, (4) our measured (ϵ mean) for both set of contours, (5) our measured (ϵ profile) outward from the cluster center for both set of contours, (6) provided dynamical classification by the works considered, (7) list of authors.

Table A.6. Comparison of mean ICM ellipticity measurements for clusters in common with other authors.

X-CLASS (1)	Other ID (2)	Dynamical State (3)	ϵ mean-a (4)	ϵ mean-b (5)	ϵ mean-c (6)
96	Abell 68	Non-Relaxed	0.27	0.34	···
97	Abell 209	Non-Relaxed	0.32	0.28	···
174	Abell 478	Relaxed	0.23	0.18	0.14
243	Abell 496	Non-Relaxed	0.15	0.18	0.06
292	···	Non-Relaxed	0.29	···	0.10
428	Abell 3558	Non-Relaxed	0.24	···	0.12
470	···	Non-Relaxed	0.20	···	0.03
706	···	Non-Relaxed	0.17	···	0.06
707	···	Relaxed	0.16	···	0.10
759	Abell 2218A	Non-Relaxed	0.19	0.21	···
836	Abell 2034	Non-Relaxed	0.19	0.15	···
1019	···	Relaxed	0.20	···	0.04
1338	Abell 907	Non-Relaxed	0.24	0.34	···
1767	···	Relaxed	0.08	0.17	···
2041	···	Non-Relaxed	0.20	···	···
2064	Abell 3395E	Non-Relaxed	0.49	···	0.23
2086	Hercules	Non-Relaxed	0.20	0.26	···
2101	···	Non-Relaxed	0.18	0.33	···
2152	Abell 1201	Non-Relaxed	0.35	0.51	···
2202	···	Non-Relaxed	0.28	0.36	···
2320	Abell 754	Non-Relaxed	0.49	···	0.20
2449	···	Non-Relaxed	0.15	0.18	···
2450	···	Non-Relaxed	0.32	0.34	···
2467	Abell 697	Non-Relaxed	0.21	0.24	···
2772	···	Relaxed	0.08	0.12	···
2842	Abell 2420	Non-Relaxed	0.26	0.20	···
2843	Abell 2426	Non-Relaxed	0.16	0.15	···
2951	MACS J1149.5	Non-Relaxed	0.23	0.30	···
2955	MACS J2214.9	Non-Relaxed	0.18	0.32	···
2976	MACS J2129.4	Non-Relaxed	0.06	0.16	···
3097	Abell 3112	Relaxed	0.22	···	0.14
3114	Abell 521	Non-Relaxed	0.28	0.27	···
3137	Zwicky 3146	Non-Relaxed	0.12	0.11	···
3150	···	Non-Relaxed	0.27	0.30	···
3153	···	Relaxed	0.13	0.21	···
3249	···	Non-Relaxed	0.18	0.20	···
3297	MACS J0717.5	Non-Relaxed	0.31	0.31	···
3337	···	Relaxed	0.07	0.13	···
3414	···	Relaxed	0.20	0.24	···
3490	Abell 133	Relaxed	0.17	0.19	0.09
20188	Abell 773	Non-Relaxed	0.21	0.22	···
20463	Abell 1914	Non-Relaxed	0.23	0.17	···
20679	Abell 1068	Relaxed	0.27	0.26	···
20682	···	Relaxed	0.10	0.11	···
20710	Abell 2667	Relaxed	0.17	0.19	···
20981	···	Relaxed	0.05	0.08	···
21325	Abell 2204	Relaxed	0.08	0.18	0.05
21391	Zwicky 2089	Relaxed	0.21	0.29	···
21601	···	Relaxed	0.18	0.29	···
22639	···	Non-Relaxed	0.22	0.19	···
22878	Abell 383	Relaxed	0.07	0.06	···
22909	···	Relaxed	0.21	0.25	···
22988	Abell 1775	Non-Relaxed	0.15	0.12	···
23095	Bullet	Non-Relaxed	0.19	0.18	···

Table A.6. continued.

X-CLASS (1)	Other ID (2)	Dynamical State (3)	ϵ mean-a (4)	ϵ mean-b (5)	ϵ mean-c (6)
23195	Abell 1835	Relaxed	0.09	0.12	···
23375	Abell 3364	Non-Relaxed	0.14	0.13	···
23388	···	Relaxed	0.07	0.05	···
23843	···	Relaxed	0.08	0.16	···
23933	Abell 780	Relaxed	0.11	0.15	···
24004	Abell 2029	Relaxed	0.22	0.20	0.11
24547	Abell 2645	Non-Relaxed	0.23	0.39	···
24615	Abell 2163	Non-Relaxed	0.21	0.24	0.08
24630	···	Non-Relaxed	0.17	0.20	···
24641	···	Relaxed	0.12	0.19	···
24645	MACS J1423.8	Relaxed	0.10	0.17	···
24690	···	Relaxed	0.05	0.09	···
24787	···	Non-Relaxed	0.19	0.34	···
24790	···	Non-Relaxed	0.18	0.21	···
24797	···	Non-Relaxed	0.13	0.25	···

Notes. (1) X-CLASS cluster ID number, (2) other ID, (3) cluster dynamical state provided by the three authors, (4) Our measured mean ellipticity, (ϵ mean-a), of the fitted ellipses to our set of ICM contours, (5) mean ellipticity, (ϵ mean-b), of the employed isophotes measured by Mantz et al. (2015), (6) mean ellipticity, (ϵ mean-c), of the x-ray flux in the cluster image measured by Parekh et al. (2015).

Appendix B: Figures

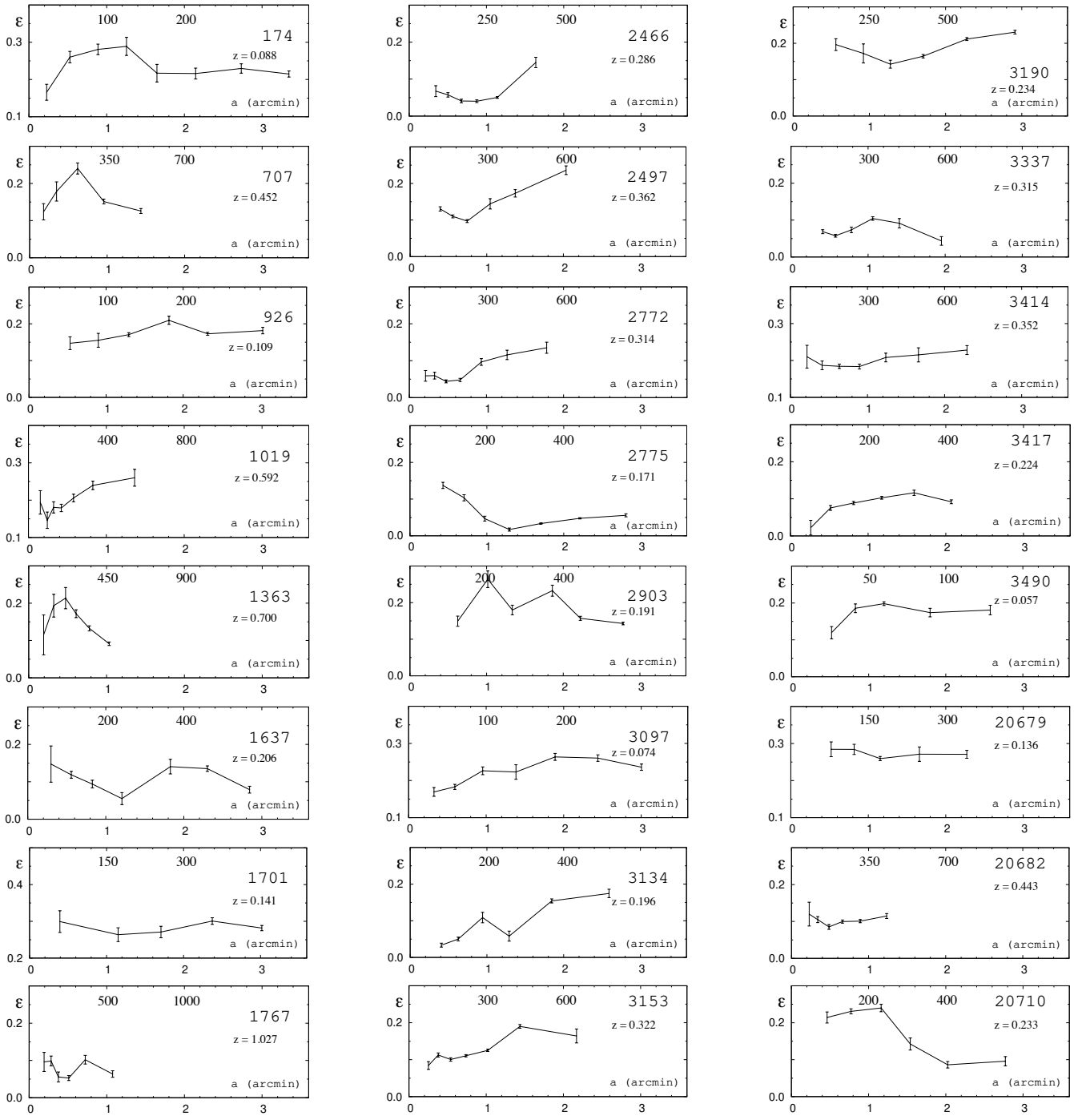

Fig. B.1. Ellipticity profiles of the 43 dynamically relaxed clusters as a function of semimajor axis (a) for the fitted ellipses to ICM contours. The error bars indicate the uncertainty in the fit of the ellipses to the x-ray contours. The upper scale is in kpc.

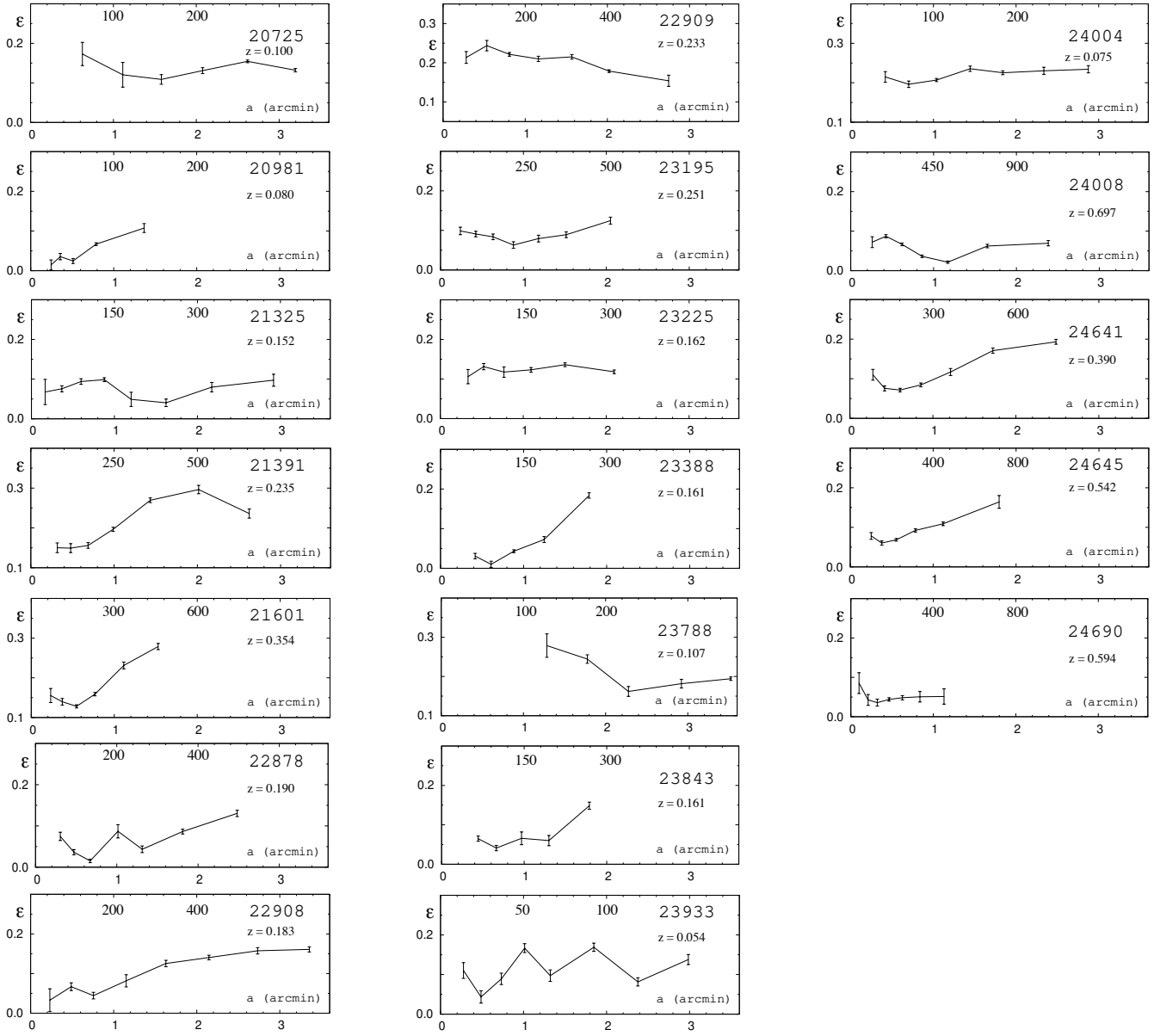

Fig. B.1. continued

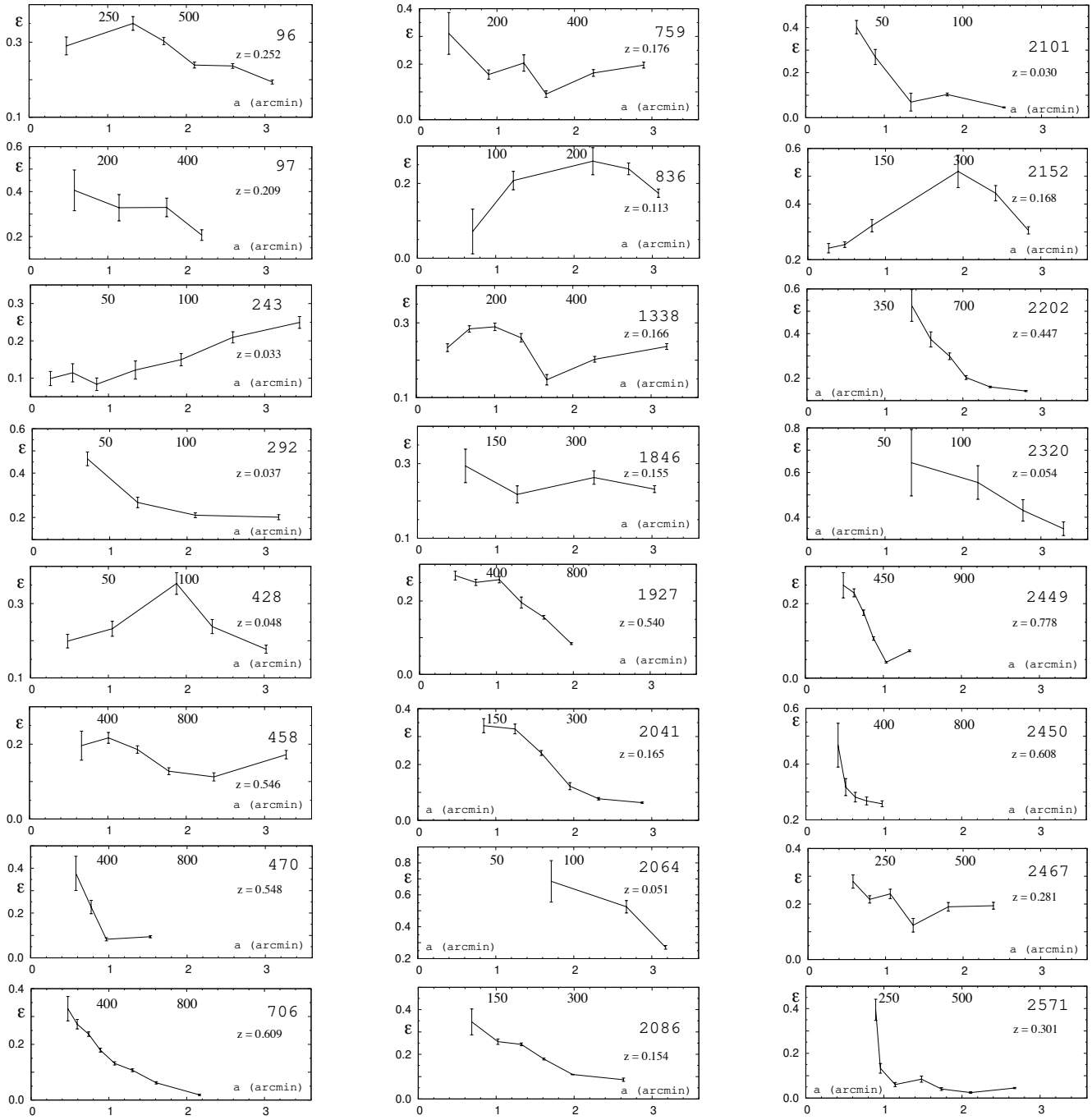

Fig. B.2. Ellipticity profiles of the 47 dynamically non-relaxed clusters.

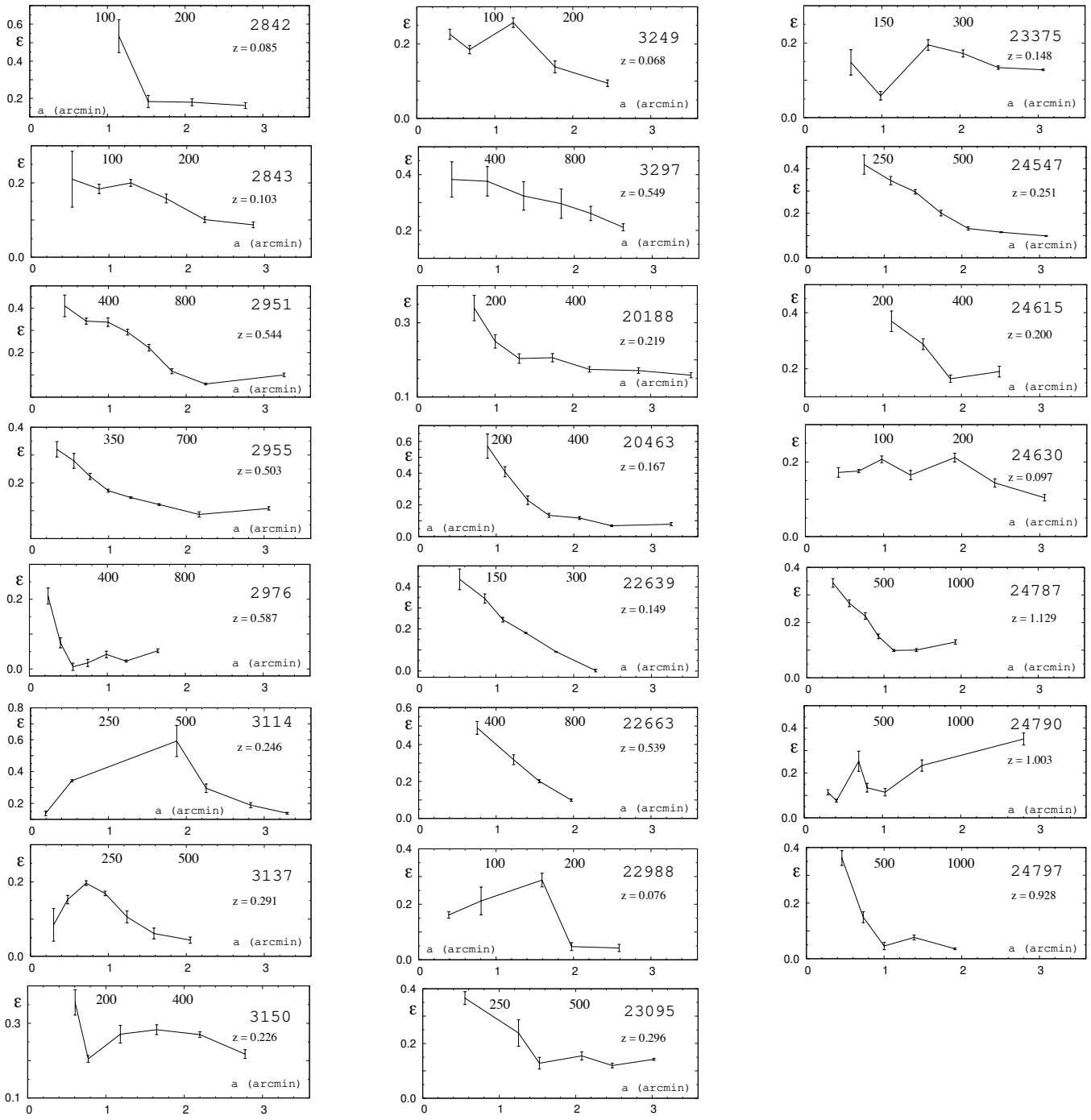

Fig. B.2. continued

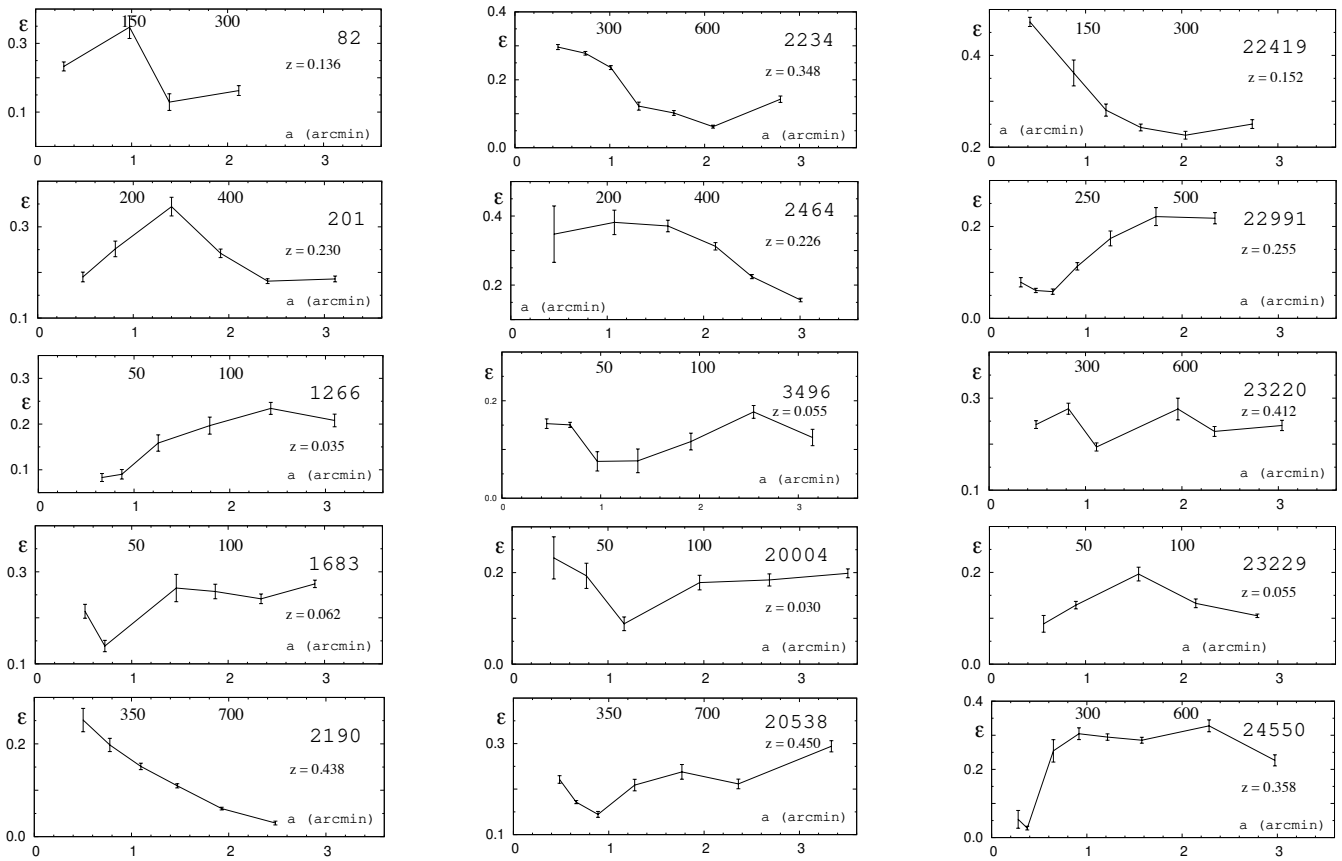

Fig. B.3. Ellipticity profiles of the 15 dynamically intermediate clusters.